

World Journal of *Gastroenterology*

World J Gastroenterol 2024 April 28; 30(16): 2179-2286



EDITORIAL

- 2179 Fecal microbiota transplantation for irritable bowel syndrome: Current evidence and perspectives
Dai C, Huang YH, Jiang M
- 2184 MicroRNAs in inflammatory bowel disease: What do we know and what can we expect?
Oliveira ECS, Quaglio AEV, Grillo TG, Di Stasi LC, Sasaki LY
- 2191 Microplastics and microbiota: Unraveling the hidden environmental challenge
Demarquoy J

REVIEW

- 2195 Mechanisms of tumor immunosuppressive microenvironment formation in esophageal cancer
Zhang XJ, Yu Y, Zhao HP, Guo L, Dai K, Lv J

MINIREVIEWS

- 2209 Laryngopharyngeal reflux disease: Updated examination of mechanisms, pathophysiology, treatment, and association with gastroesophageal reflux disease
Cui N, Dai T, Liu Y, Wang YY, Lin JY, Zheng QF, Zhu DD, Zhu XW
- 2220 Drug-induced mucosal alterations observed during esophagogastroduodenoscopy
Iwamura M, Kawano S, Otsuka M

ORIGINAL ARTICLE**Retrospective Study**

- 2233 Preoperative prediction of perineural invasion of rectal cancer based on a magnetic resonance imaging radiomics model: A dual-center study
Liu Y, Sun BJT, Zhang C, Li B, Yu XX, Du Y

Observational Study

- 2249 Association between childhood obesity and gut microbiota: 16S rRNA gene sequencing-based cohort study
Li XM, Lv Q, Chen YJ, Yan LB, Xiong X

Basic Study

- 2258 Chitin-glucan improves important pathophysiological features of irritable bowel syndrome
Valibouze C, Dubuquoy C, Chavatte P, Genin M, Maquet V, Modica S, Desreumaux P, Rousseaux C

- 2272 Optimization of tracheoesophageal fistula model established with T-shaped magnet system based on magnetic compression technique

Zhang MM, Mao JQ, Shen LX, Shi AH, Lyu X, Ma J, Lyu Y, Yan XP

LETTER TO THE EDITOR

- 2281 Ability of *Helicobacter pylori* to internalize into *Candida*

Chen ZH, Sun JC, Yang TX, Cui GZ

- 2285 Transjugular intrahepatic portosystemic shunt: A promising therapy for recompensation in cirrhotic patients

Jin YN, Zhang W

ABOUT COVER

Editorial Board Member of *World Journal of Gastroenterology*, Zhao-Hui Huang, MD, Director, Professor, Wuxi Cancer Institute, Affiliated Hospital of Jiangnan University, Wuxi 214062, Jiangsu Province, China.
hzhwxsy@126.com

AIMS AND SCOPE

The primary aim of *World Journal of Gastroenterology* (*WJG*, *World J Gastroenterol*) is to provide scholars and readers from various fields of gastroenterology and hepatology with a platform to publish high-quality basic and clinical research articles and communicate their research findings online. *WJG* mainly publishes articles reporting research results and findings obtained in the field of gastroenterology and hepatology and covering a wide range of topics including gastroenterology, hepatology, gastrointestinal endoscopy, gastrointestinal surgery, gastrointestinal oncology, and pediatric gastroenterology.

INDEXING/ABSTRACTING

The *WJG* is now abstracted and indexed in Science Citation Index Expanded (SCIE), MEDLINE, PubMed, PubMed Central, Scopus, Reference Citation Analysis, China Science and Technology Journal Database, and Superstar Journals Database. The 2023 edition of Journal Citation Reports® cites the 2022 impact factor (IF) for *WJG* as 4.3; Quartile category: Q2. The *WJG*'s CiteScore for 2021 is 8.3.

RESPONSIBLE EDITORS FOR THIS ISSUE

Production Editor: *Yu-Xi Chen*; Production Department Director: *Xiang Li*; Cover Editor: *Jia-Ru Fan*.

NAME OF JOURNAL

World Journal of Gastroenterology

ISSN

ISSN 1007-9327 (print) ISSN 2219-2840 (online)

LAUNCH DATE

October 1, 1995

FREQUENCY

Weekly

EDITORS-IN-CHIEF

Andrzej S Tarnawski

EXECUTIVE ASSOCIATE EDITORS-IN-CHIEF

Xian-Jun Yu (Pancreatic Oncology), Jian-Gao Fan (Chronic Liver Disease), Hou-Bao Liu (Biliary Tract Disease)

EDITORIAL BOARD MEMBERS

<http://www.wjgnet.com/1007-9327/editorialboard.htm>

PUBLICATION DATE

April 28, 2024

COPYRIGHT

© 2024 Baishideng Publishing Group Inc

PUBLISHING PARTNER

Shanghai Pancreatic Cancer Institute and Pancreatic Cancer Institute, Fudan University
Biliary Tract Disease Institute, Fudan University

INSTRUCTIONS TO AUTHORS

<https://www.wjgnet.com/bpg/gerinfo/204>

GUIDELINES FOR ETHICS DOCUMENTS

<https://www.wjgnet.com/bpg/GerInfo/287>

GUIDELINES FOR NON-NATIVE SPEAKERS OF ENGLISH

<https://www.wjgnet.com/bpg/gerinfo/240>

PUBLICATION ETHICS

<https://www.wjgnet.com/bpg/GerInfo/288>

PUBLICATION MISCONDUCT

<https://www.wjgnet.com/bpg/gerinfo/208>

POLICY OF CO-AUTHORS

<https://www.wjgnet.com/bpg/GerInfo/310>

ARTICLE PROCESSING CHARGE

<https://www.wjgnet.com/bpg/gerinfo/242>

STEPS FOR SUBMITTING MANUSCRIPTS

<https://www.wjgnet.com/bpg/GerInfo/239>

ONLINE SUBMISSION

<https://www.f6publishing.com>

PUBLISHING PARTNER'S OFFICIAL WEBSITE

<https://www.shca.org.cn>
<https://www.zs-hospital.sh.cn>

Retrospective Study

Preoperative prediction of perineural invasion of rectal cancer based on a magnetic resonance imaging radiomics model: A dual-center study

Yan Liu, Bai-Jin-Tao Sun, Chuan Zhang, Bing Li, Xiao-Xuan Yu, Yong Du

Specialty type: Gastroenterology and hepatology**Provenance and peer review:**

Unsolicited article; Externally peer reviewed.

Peer-review model: Single blind**Peer-review report's scientific quality classification**Grade A (Excellent): 0
Grade B (Very good): B
Grade C (Good): 0
Grade D (Fair): 0
Grade E (Poor): 0**P-Reviewer:** Engin G, Turkey**Received:** January 2, 2024**Peer-review started:** January 2, 2024**First decision:** January 31, 2024**Revised:** February 8, 2024**Accepted:** March 20, 2024**Article in press:** March 20, 2024**Published online:** April 28, 2024**Yan Liu, Bai-Jin-Tao Sun, Chuan Zhang, Bing Li, Xiao-Xuan Yu**, Department of Radiology, The Affiliated Hospital of North Sichuan Medical College, Nanchong 637000, Sichuan Province, China**Yong Du**, Department of Radiology, The Affiliated Hospital of North Sichuan Medical College, Nanchong 637000, Sichuan Province, China. duyong@nsmc.edu.cn**Corresponding author:** Yong Du, MD, Professor, Department of Radiology, The Affiliated Hospital of North Sichuan Medical College, No. 1 Maoyuannan Road, Nanchong 637000, Sichuan Province, China. duyong@nsmc.edu.cn

Abstract

BACKGROUND

Perineural invasion (PNI) has been used as an important pathological indicator and independent prognostic factor for patients with rectal cancer (RC). Preoperative prediction of PNI status is helpful for individualized treatment of RC. Recently, several radiomics studies have been used to predict the PNI status in RC, demonstrating a good predictive effect, but the results lacked generalizability. The preoperative prediction of PNI status is still challenging and needs further study.

AIM

To establish and validate an optimal radiomics model for predicting PNI status preoperatively in RC patients.

METHODS

This retrospective study enrolled 244 postoperative patients with pathologically confirmed RC from two independent centers. The patients underwent preoperative high-resolution magnetic resonance imaging (MRI) between May 2019 and August 2022. Quantitative radiomics features were extracted and selected from oblique axial T2-weighted imaging (T2WI) and contrast-enhanced T1WI (T1CE) sequences. The radiomics signatures were constructed using logistic regression analysis and the predictive potential of various sequences was compared (T2WI, T1CE and T2WI + T1CE fusion sequences). A clinical-radiomics (CR) model was established by combining the radiomics features and clinical risk factors. The internal and external validation groups were used to validate the

proposed models. The area under the receiver operating characteristic curve (AUC), DeLong test, net reclassification improvement (NRI), integrated discrimination improvement (IDI), calibration curve, and decision curve analysis (DCA) were used to evaluate the model performance.

RESULTS

Among the radiomics models, the T2WI + T1CE fusion sequences model showed the best predictive performance, in the training and internal validation groups, the AUCs of the fusion sequence model were 0.839 [95% confidence interval (CI): 0.757-0.921] and 0.787 (95%CI: 0.650-0.923), which were higher than those of the T2WI and T1CE sequence models. The CR model constructed by combining clinical risk factors had the best predictive performance. In the training and internal and external validation groups, the AUCs of the CR model were 0.889 (95%CI: 0.824-0.954), 0.889 (95%CI: 0.803-0.976) and 0.894 (95%CI: 0.814-0.974). Delong test, NRI, and IDI showed that the CR model had significant differences from other models ($P < 0.05$). Calibration curves demonstrated good agreement, and DCA revealed significant benefits of the CR model.

CONCLUSION

The CR model based on preoperative MRI radiomics features and clinical risk factors can preoperatively predict the PNI status of RC noninvasively, which facilitates individualized treatment of RC patients.

Key Words: Rectal cancer; Perineural invasion; Magnetic resonance imaging; Radiomics; Nomogram

©The Author(s) 2024. Published by Baishideng Publishing Group Inc. All rights reserved.

Core Tip: We constructed radiomics predictive models, clinical predictive model and clinical-radiomics (CR) model based on preoperative magnetic resonance imaging images of rectal cancer (RC), and independent clinical risk factors, to predict the preoperative perineural invasion (PNI) status of RC patients. The reliability and repeatability of the established predictive models were analyzed using internal and external validation groups. The CR model had the best stable neutral performance in both the internal and external validation groups. Therefore, the CR model was able to predict the PNI status of RC noninvasively before surgery, thereby providing support for the individualized treatment of RC patients.

Citation: Liu Y, Sun BJT, Zhang C, Li B, Yu XX, Du Y. Preoperative prediction of perineural invasion of rectal cancer based on a magnetic resonance imaging radiomics model: A dual-center study. *World J Gastroenterol* 2024; 30(16): 2233-2248

URL: <https://www.wjgnet.com/1007-9327/full/v30/i16/2233.htm>

DOI: <https://dx.doi.org/10.3748/wjg.v30.i16.2233>

INTRODUCTION

Rectal cancer (RC) is one of the most common gastrointestinal malignancies worldwide, and its incidence is increasing annually. Most patients with RC are diagnosed in the middle and late stages[1]. Perineural invasion (PNI), a potential pathway for the metastatic spread of RC, has been used as an important pathological indicator and independent prognostic factor for patients with RC since the 7th edition of the cancer staging system developed by the American Joint Commission on Cancer (AJCC)[2].

PNI refers to the invasion of nerves by tumor cells, followed by the spread of tumor cells along the nerve sheath. It is categorized as tumor cell invasion of endoneural, neuronal sheath, and epineural membrane layers, or tumor cells surrounding the nerve and wrapping around > 33% of the epineural membrane[3]. Multiple studies have shown that the PNI status is correlated with postoperative recurrence rates and poor prognosis of RC[4-8]. Preoperative stratification of RC patients according to the PNI status facilitates individualized treatment and improves the prognosis of RC patients. Studies have shown that neoadjuvant chemoradiotherapy (nCRT) can significantly reduce the incidence of PNI[9-12]. Preoperative assessment of PNI is helpful in decision-making regarding nCRT, especially in patients with stage II RC. Currently, the use of nCRT for stage II patients is controversial. Stage II RC is a heterogeneous disease; therefore, distinct clinicopathological features may lead to different clinical outcomes and should be treated differently[13]. The latest European Society of Medical Oncology RC Guidelines indicate that PNI is a key factor in determining whether stage II patients will benefit from nCRT and postoperative adjuvant chemotherapy[14,15]. In addition, nCRT combined with total mesorectum excision is regarded as the standard treatment for locally advanced RC. Although the local recurrence rate is reduced to < 10%, the distant metastasis rate is still more than 20%-30%. Postoperative adjuvant chemotherapy is used to prevent distant metastasis, and the PNI status is an indicator of postoperative adjuvant chemotherapy[14-16]. However, nCRT can significantly reduce the incidence of PNI in patients with RC, promoting the downward phase of the tumor. Therefore, the postoperative pathological conditions do not fully reflect the patient's status[17]. The preoperative evaluation of PNI is helpful for guiding the use of postoperative adjuvant chemotherapy for patients with locally advanced RC.

Currently, PNI status cannot be assessed based on conventional preoperative biopsy or magnetic resonance imaging (MRI), but can only be determined through postoperative pathological examination. Conventional preoperative biopsy only obtains the mucosal and submucosal layers, whereas peripheral nerves mostly exist outside the mucosal muscle layer or even outside the intestinal wall. Additionally, MRI cannot display small nerves. The efficiency and timeliness of postoperative pathological testing limit the use of PNI[13].

Radiomics can extract quantitative features that reflect tumor heterogeneity, allowing the extraction of deep mining data from images and analyzing noninvasive clinical predictors to provide detailed information for personalized treatment and patient management[18]. This technique is widely used for auxiliary diagnosis, pathological staging, prediction of treatment outcomes, and prognostication. Several radiomics studies have been used to predict PNI status in RC, demonstrating a good predictive effect. However, most studies were based on computed tomography or single sequences of MRI and were conducted at single centers without external validation. Therefore, the results lacked generalizability[13,19-23].

This two-center study aimed to construct a radiomics prediction model for the PNI status of RC based on T2-weighted imaging (T2WI) and contrast-enhanced T1WI (T1CE) sequences of high-resolution MRI and to systematically compare the performance of different radiomics predictive models. The optimal radiomics predictive model combined with PNI-related clinical features was selected to construct the final clinical-radiomics (CR) model, which provided the basis for individualized management strategies for RC patients.

MATERIALS AND METHODS

Patients

This two-center retrospective study was approved by the Ethical Review Committee of the Affiliated Hospital of North Sichuan Medical College (AHNSMC, file number: 2022ER431-1), which waived the need for informed consent from participants.

The study inclusion criteria were: (1) Postoperative pathologically confirmed RC; (2) high-resolution contrast-enhanced MRI of rectum performed using 1.5 T MRI within 1 wk before the operation, and a complete TNM staging report was obtained; and (3) preoperative peripheral blood carcinoembryonic antigen (CEA) and carbohydrate antigen 19-9 (CA19-9) levels were detected within 1 wk before the operation.

The exclusion criteria included: (1) nCRT and other antitumor treatments were administered preoperatively; (2) postoperative pathological report did not record the PNI status; and (3) poor image quality, which made it difficult to segment the image of the lesion.

A total of 613 patients who underwent surgical resection of rectal RC were recruited between May 2019 and August 2022. Finally, 244 patients from two independent centers were enrolled. Among them, 170 consecutive patients from Center 1 (Affiliated Hospital of North Sichuan Medical College) were randomly divided into a training group ($n = 118$) and an internal validation group ($n = 52$) at a ratio of 7:3, whereas 74 consecutive patients from Center 2 (Second Clinical School of North Sichuan Medical College) served as an external validation group. The detailed workflow of the study is presented in [Figure 1](#).

Preoperative information on clinical and radiological variables was collected retrospectively from our medical records and Picture Archiving and Communication System (PACS). The clinical variables included age, gender, CEA level (< 5 or ≥ 5 ng/mL), CA19-9 level (< 30 or ≥ 30 U/mL), histopathological grade, and clinical M stage. The radiological variables included the distance between the tumor and anal margin, MRI T stage, MRI N (mN) stage, clinical TNM (cTNM) stage, MRI-based circumferential resection margin (mCRM), and MRI-based extramural vascular invasion (mEMVI). PNI status data were derived from postoperative pathological analysis of hematoxylin and eosin (HE)-stained sections and immunohistochemical analysis of the resected specimens.

MRI

All patients in Center 1 were scanned using Siemens Aera 1.5 T MRI, and all patients in Center 2 were scanned using GE Sigma HDxt 1.5 T MRI. The sequences included high-resolution oblique axial T2WI and axial T1CE. T1CE sequences were obtained after intravenous administration of gadolinium contrast agent using an MRI-compatible power injector at a rate of 2 mL/s and a dose of 0.2 mL/kg, followed by flushing 20 mL of saline using a high-pressure syringe. The detailed sequence parameters are presented in [Table 1](#).

Imaging analysis and segmentation

MR images were derived from PACS in the Digital Imaging and Communications in Medicine format. Two experienced radiologists, with 8 and 10 years of work experience, independently evaluated the MR images while being blinded to the postoperative pathological findings. Discrepancies among the readers were resolved through discussion. The diagnostic methods were based on the 8th AJCC staging system[24].

In cases with unknown pathological findings, Reader 1 used the 3D slicer software (version 4.11.2; <https://www.slicer.org>) to manually delineate the lesion layer-by-layer on oblique axial T2WI and axial T1CE sequences, thereby obtaining the volume of interest (VOI) of the tumor. Subsequently, the 3D mask of the tumor was exported. One month after completing the image segmentation of all patients by Reader 1, 30 patients were randomly selected, for whom Readers 1 and 2 independently performed repeated segmentation of the lesion and output masks. Repeatability analysis was conducted within and between observers to evaluate the stability of subsequent radiomics features.

Table 1 Magnetic resonance imaging parameters of each sequence

Scanner	Sequence	Orientation	TR (ms)	TE (ms)	FOV (mm ²)	Matrix	Thickness (mm)
Siemens Aera 1.5T	T2WI	Oblique axial	4480	87	190 × 190	320 × 320	3
	T1CE	Oblique axial	7	3	210 × 210	256 × 256	3
GE Signa HDxt 1.5T	T2WI	Oblique axial	4120	70	180 × 180	256 × 192	3
	T1CE	Oblique axial	6	3	200 × 200	288 × 160	3

TR: Repetition time; TE: Echo time; FOV: Field of view; T2WI: T2-weighted imaging; T1CE: Contrast-enhanced T1WI.

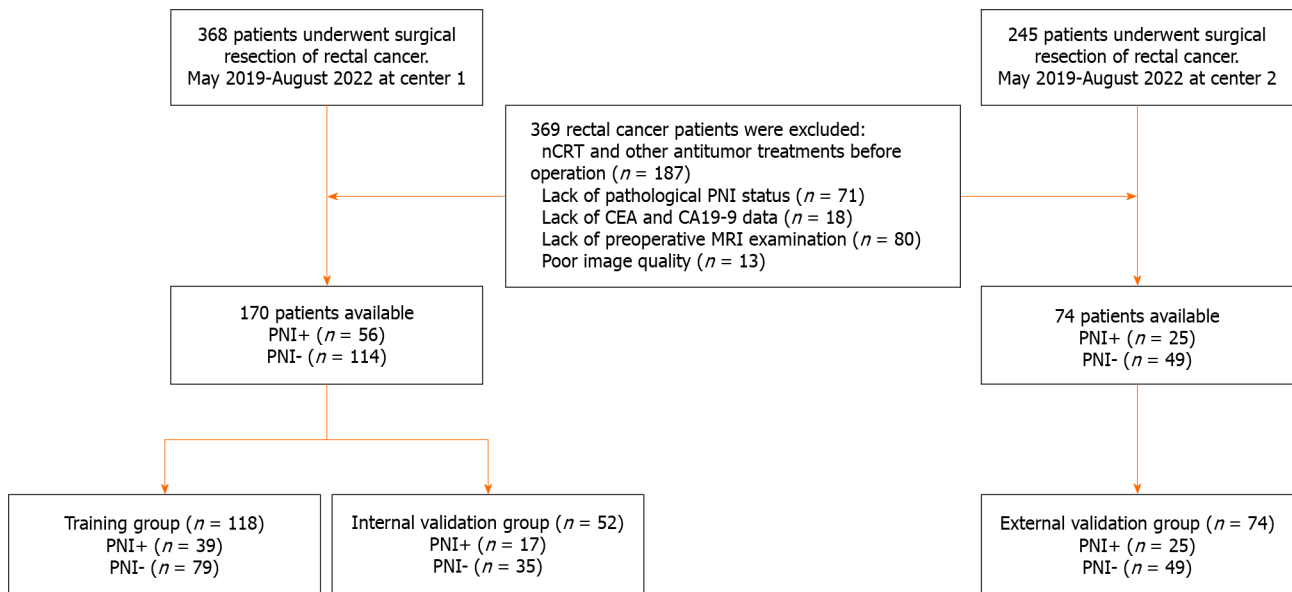


Figure 1 Flowchart of participant selection. nCRT: Neoadjuvant chemoradiotherapy; CEA: Carcinoembryonic antigen; CA19-9: Carbohydrate antigen 19-9; MRI: Magnetic resonance imaging; PNI: Perineural invasion.

Radiomics feature extraction and selection

The Radiomics package of the 3D-Slicer software (version 4.11.2; <https://www.slicer.org>) was used for original image preprocessing and radiomics feature extraction. To minimize the image extraction of radiomics features using different MRI models, the preprocessing of the original images included the following steps: (1) Voxel spacing was standardized, and all images were resampled to a volume of 1 mm × 1 mm × 1 mm; and (2) the image noise and normalized voxel intensity were controlled, and the voxel intensity values were discretized using a fixed bin width (25 HU)[25].

All VOIs were imported into the 3D-Slicer software for feature extraction. In total, 944 radiomics features were extracted for each VOI. The image types of the extracted radiomics features included the following: (1) A total of 107 radiomics features extracted from the original image after image preprocessing [including shape features, first-order statistical features, gray-level co-occurrence matrix (GLCM) features, gray-level dependence matrix features, gray-level run length matrix (GLRLM) features, gray-level size zone matrix (GLSZM) features, and neighboring gray tone difference matrix features]; (2) a total of 93 radiomics features of images extracted (including first-order statistical, GLCM, gray-level dependence matrix, GLRLM, GLSZM, and neighboring gray tone difference matrix) using the Laplace operator of the Gaussian filter and the image derived from the transformation of 1σ (0.5); and (3) a total of 744 radiomics features extracted from eight image types derived from wavelet transformation (including first-order statistical features, GLCM features, gray-level dependence matrix features, GLRLM features, GLSZM features, and neighboring gray tone difference matrix features). The specific radiomics feature types extracted based on the abovementioned images are shown in [Supplementary Table 1](#). For further details, please refer to <http://pyradiomics.readthedocs.io/en/Latest/features.html>.

Based on the training group data, the radiomics features were reduced and screened. First, dimensionality reduction, Z-score standardization, and maximum-minimum normalization of radiomics eigenvalues were used to remove irrelevant and redundant features. Then, radiomics features were screened using the following steps: (1) Radiomics features with inter- and intraclass correlation coefficients > 0.75 were screened to ensure their stability; (2) radiomics features with significant differences ($P < 0.05$) were screened using univariate logistic regression analysis; and (3) the least absolute shrinkage and selection operator regression algorithm was used to adjust the penalty parameters using 10-fold crossvalidation, and the regression coefficients of each radiomics feature were compressed, according to the principle of the simplest model. The radiomics features with non-zero coefficients were screened to establish the Rad-score.

Model construction and evaluation

Based on the training group data, univariate logistic regression analysis was carried out for all clinical and MRI factors. According to our results and clinical practice, relevant factors were selected for multifactorial logistic regression analysis. We constructed a clinical predictive model and three radiomics predictive models, namely T2WI, T1CE and T2WI + T1CE fusion sequence. Finally, the best radiomics predictive model was selected and combined with selected clinical and MRI risk factors to construct a combined CR predictive model.

The above predictive models were tested in the internal and external validation groups to determine their differentiation, calibration and clinical effectiveness. The area under the receiver operating characteristic (ROC) curve (AUC), Delong test, net reclassification improvement (NRI) and integrated discrimination improvement (IDI) were used to compare the differentiation of each predictive model. Calibration curves were used to evaluate the calibration degree of each predictive model; that is, the consistency between the predicted and actual results. Decision curve analysis (DCA) was used to evaluate the efficacy of each predictive model. Finally, the optimal model was selected to construct a nomogram and an online interactive nomogram. The detailed research process is presented in [Figure 2](#).

Statistical analysis

The clinical and MRI factors were analyzed using SPSS software version 26.0. Categorical variables are expressed as percentages and analyzed using χ^2 or Fisher's exact tests. Continuous variables with normal data distribution were expressed as mean \pm SD, whereas those with non-normal distribution were expressed as median (interquartile range). $P < 0.05$ (two-tailed) was considered statistically significant. R version 4.2.1 was used for feature screening, construction and evaluation of the predictive models. Several R packages were used for data analysis, including caret, irr, car, MASS, glmnet, pROC, nricens, rms, DynNom, rconnect, rmda, plot, and ggplot2.

RESULTS

Patient characteristics

In this study, two hundred and forty-four patients were enrolled and categorized into the training ($n = 118$), internal validation ($n = 52$) and external validation ($n = 74$) groups. [Table 2](#) summarizes the detailed clinical and radiological characteristics of the patients. There were no significant differences in the proportion of PNI-positive patients between the training group and the two validation groups (32.1, 32.7 and 33.8%, respectively; $P > 0.05$). There were no significant differences between the training, internal validation and external validation datasets ($P > 0.05$). In contrast, the training group dataset demonstrated significant differences between PNI-positive and PNI-negative patients in terms of CA19-9 level, mN, mCRM, mEMVI and histological grade ($P < 0.05$). In the internal validation group, there were significant differences in the CEA and CA19-9 levels between the PNI-positive and PNI-negative patients ($P < 0.05$). In the external validation group, there were significant differences in CEA, mN and mEMVI between the PNI-positive and PNI-negative patients ($P < 0.05$).

Model construction and evaluation

In this study, twelve features were retained from the three sequences: T2WI ($n = 5$), T1CE ($n = 2$) and T2WI + T1CE fusion sequence ($n = 5$). The detailed information regarding these features is presented in [Figure 3](#) and [Supplementary Table 2](#). The radiomics scores were calculated by multiplying the selected features with the corresponding coefficients for each modality as follows: T2WI_Rad-score = $14.86872 + (0.03702 \times \text{original_glcm_Correlation}) + (0.10289 \times \text{original_glcm_MCC}) + (8.2082 \times \text{original_glszm_ZoneEntropy}) + (9.15542 \times \text{wavelet-LLL_glcm_MCC}) + (-3.61471 \times \text{wavelet-LLL_gllm_GrayLevelNonUniformityNormalized})$. T1CE_Rad-score = $-26.133 + (2.919 \times \text{original_shape_Maximum^DDiameterSlice}) + (22.566 \times \text{original_gldm_DependenceEntropy})$. (T2WI + T1CE)_Rad-score = $-7.0772 + (-0.1798 \times \text{T2WI_original_glcm_MCC}) + (0.7251 \times \text{T2WI_original_glszm_ZoneEntropy}) + (7.5941 \times \text{T2WI_wavelet-LLL_glcm_MCC}) + (-4.442 \times \text{T2WI_wavelet-LLL_gllm_GrayLevelNonUniformityNormalized}) + (2.3265 \times \text{T1CE_original_shape_Maximum^DDiameterSlice})$.

Three radiomics predictive models were constructed based on the Rad-score using logistic regression. In the training group, the AUCs of the T2WI sequence radiomics predictive model, T1CE sequence radiomics predictive model, and T2WI + T1CE fusion sequence radiomics predictive model were 0.817, 0.798 and 0.839, respectively, and these values were 0.763, 0.689 and 0.787 in the internal validation group, respectively, and 0.759, 0.841, and 0.836 in the external validation group, respectively. Detailed information regarding the predictive models is presented in [Table 3](#) and [Figure 4](#).

Univariate and multivariate logistic regression analyses of training group data demonstrated that cTNM [odds ratio (OR): 42.002; 95% confidence interval (CI): 2.913-605.511] ($P = 0.006$) and histological grade (OR: 0.113; 95%CI: 0.020-0.658) ($P = 0.015$) were independent risk factors for PNI in RC. Further details are presented in [Table 4](#). The AUCs of the clinical predictive models for the training, internal validation and external validation groups were 0.804, 0.828 and 0.813, respectively. Further details are presented in [Table 3](#).

The Delong test for the training group data showed no significant differences among the three radiomics predictive models ($P = 0.476$). However, the NRI and IDI indices demonstrated that the T2WI + T1CE fusion sequence radiomics predictive model had significantly higher predictive ability compared to the T2WI and T1CE sequence radiomics predictive models (NRI index > 0 , IDI index > 0 , $P < 0.05$). The T2WI + T1CE fusion sequence radiomics predictive model was superior to the T2WI and T1CE sequence radiomics predictive models. Further details are presented in [Table 5](#). The T2WI + T1CE_Rad-score and independent clinical risk factors (cTNM and histological grade) were selected to construct a

Table 2 Characteristics of patients in the training, internal validation and external validation groups, n (%)

Characteristics	Training group (n = 118)		P value	Internal validation group (n = 52)		P value	External validation group (n = 74)		P value
	PNI+ (n = 39)	PNI- (n = 79)		PNI+ (n = 17)	PNI- (n = 35)		PNI+ (n = 25)	PNI- (n = 49)	
Sex			0.854			0.882			0.640
Male	25 (64.1)	52 (65.8)		12 (70.6)	24 (68.6)		16 (64.0)	34 (69.4)	
Female	14 (35.9)	27 (34.2)		5 (29.4)	11 (31.4)		9 (36.0)	15 (30.6)	
Age (yr)	68 (56.5-73)	68 (58.5-75)	0.479	66.59 ± 12.57	64.17 ± 10.32	0.497	65.24 ± 11.70	66.84 ± 9.85	0.562
CEA			0.150			0.027			0.005
Negative (< 5 ng/mL)	23 (59.0)	57 (72.2)		9 (52.9)	30 (85.7)		14 (56.0)	42 (85.7)	
Positive (≥ 5 ng/mL)	16 (41.0)	22 (27.8)		8 (47.1)	5 (14.3)		11 (44.0)	7 (14.3)	
CA19-9			0.034			0.019			1.000
Negative (< 30 U/mL)	30 (76.9)	72 (91.1)		12 (70.6)	34 (97.1)		23 (92.0)	46 (93.9)	
Positive (≥ 30 U/mL)	9 (23.1)	7 (8.9)		5 (29.4)	1 (2.9)		2 (8.0)	3 (6.1)	
DIS			0.050			0.444			0.823
High	24 (61.5)	31 (39.2)		9 (52.9)	15 (42.9)		12 (48.0)	22 (44.9)	
Mid	3 (7.7)	16 (20.3)		5 (29.4)	9 (25.7)		5 (20.0)	13 (26.5)	
Low	12 (30.8)	32 (40.5)		3 (17.6)	11 (31.4)		8 (32.0)	14 (28.6)	
mT			0.211			0.885			0.314
mT1-2	3 (7.7)	15 (19.0)		6 (35.3)	10 (28.6)		5 (20.0)	9 (18.4)	
mT3	24 (61.5)	47 (59.5)		8 (47.1)	18 (51.4)		14 (56.0)	32 (65.3)	
mT4	12 (30.8)	17 (21.5)		3 (17.6)	7 (20.0)		6 (24.0)	8 (16.3)	
mN			0.003			0.063			0.028
mN0	5 (12.8)	27 (34.2)		3 (17.6)	18 (51.4)		6 (24.0)	19 (38.8)	
mN1	13 (33.3)	33 (41.8)		5 (29.4)	7 (20.0)		7 (28.0)	21 (42.9)	
mN2	21 (53.8)	19 (24.1)		9 (52.9)	10 (28.6)		12 (48.0)	9 (18.4)	
cM			0.070			1.000			0.064
cM0	34 (87.2)	77 (97.5)		17 (100.0)	34 (97.1)		22 (88.0)	49 (100.0)	
cM1	5 (12.8)	2 (2.5)		0 (0.0)	1 (2.9)		3 (12.0)	0 (0.0)	
cTNM			1.000			1.000			1.000
I	1 (2.6)	29 (36.7)		0 (0.0)	16 (45.7)		0 (0.0)	18 (36.7)	
II	9 (23.1)	25 (31.6)		5 (29.4)	13 (37.1)		3 (12.0)	12 (24.5)	
III	25 (64.1)	23 (29.1)		11 (64.7)	5 (14.3)		19 (76.0)	19 (38.8)	
IV	4 (10.3)	2 (2.5)		1 (5.9)	1 (2.9)		3 (12.0)	0 (0.0)	
mCRM			0.002			0.374			0.236
Negative	14 (35.9)	52 (65.8)		9 (52.9)	23 (65.7)		15 (60.0)	36 (73.5)	
Positive	25 (64.1)	27 (34.2)		8 (47.1)	12 (34.3)		10 (40.0)	13 (26.5)	
mEMVI			0.016			0.935			0.009
Negative	15 (38.5)	49 (62.0)		10 (58.8)	21 (60.0)		10 (40.0)	35 (71.4)	
Positive	24 (61.5)	30 (38.0)		7 (41.2)	14 (40.0)		15 (60.0)	14 (28.6)	
Histological grade			0.000			0.920			0.894

Well differentiated	4 (10.3)	27 (34.2)	2 (11.8)	11 (31.4)	4 (16.0)	13 (26.5)
Moderately differentiated	26 (66.7)	49 (62.0)	12 (70.6)	23 (65.7)	18 (72.0)	34 (69.4)
Poorly differentiated	9 (23.1)	3 (3.8)	3 (17.6)	1 (2.9)	3 (12.0)	2 (4.1)

P value represents analysis of PNI-positive and PNI-negative datasets between each group. PNI: Perineural infiltration; CEA: Carcinoembryonic antigen; CA19-9: Carbohydrate antigen 19-9; mCRM: MRI-based circumferential resection margin; mEMVI: MRI-based extramural vascular invasion; mT: MRI T stage; mN: MRI N stage; cM: Clinical M stage; cTNM: Clinical TNM stage; DIS: The distance between tumor and anal margin, Low (0-5 cm from the anal verge), middle (5.1-10 cm from the anal verge), and high (10.1-15 cm from the anal verge).

Table 3 Performance of various predictive models in the training, internal validation and external validation groups

Models	Training group	Internal validation group	External validation group
T2WI			
AUC (95%CI)	0.817 (0.733-0.901)	0.763 (0.626-0.900)	0.759 (0.644-0.875)
Sensitivity	0.564	0.294	0.480
Specificity	0.899	0.886	0.857
Positive predictive value	0.733	0.556	0.632
Negative predictive value	0.807	0.721	0.764
T1CE			
AUC (95%CI)	0.798 (0.707-0.890)	0.689 (0.521-0.857)	0.841 (0.752-0.930)
Sensitivity	0.487	0.471	0.480
Specificity	0.937	0.857	0.878
Positive predictive value	0.792	0.615	0.667
Negative predictive value	0.787	0.769	0.768
T2WI + T1CE			
AUC (95%CI)	0.839 (0.757-0.921)	0.787 (0.650-0.923)	0.836 (0.735-0.937)
Sensitivity	0.641	0.529	0.560
Specificity	0.899	0.914	0.939
Positive predictive value	0.758	0.750	0.824
Negative predictive value	0.835	0.800	0.807
Clinical model			
AUC (95%CI)	0.804 (0.727-0.881)	0.828 (0.719-0.937)	0.813 (0.724-0.903)
Sensitivity	0.718	0.706	0.800
Specificity	0.747	0.829	0.694
Positive predictive value	0.583	0.667	0.571
Negative predictive value	0.843	0.829	0.872
CR model			
AUC (95%CI)	0.889 (0.824-0.954)	0.889 (0.803-0.976)	0.894 (0.814-0.974)
Sensitivity	0.692	0.647	0.760
Specificity	0.924	0.886	0.899
Positive predictive value	0.818	0.733	0.792
Negative predictive value	0.859	0.838	0.880

T2WI: T2-weighted imaging; T1CE: Contrast-enhanced T1WI; CR: Clinical-radiomics prediction model; AUC: Area under receiver operating characteristic curve.

Table 4 Results of univariate and multivariate logistic regression analyses

Variables	Univariate logistic regression		Multivariate logistic regression	
	OR (95%CI)	P value	OR (95%CI)	P value
Gender	0.927 (0.418-2.098)	0.854	NA	NA
Age	0.976 (0.944-1.008)	0.138	NA	NA
CEA	1.802 (0.801-4.045)	0.152	NA	NA
CA19-9	3.086 (1.056-9.375)	0.040 ^a	NA	NA
DIS	1.487 (0.968-2.329)	0.075	NA	NA
mT	1.717 (0.919-3.312)	0.096	NA	NA
mN	2.507 (1.467-4.495)	0.001 ^a	NA	NA
cM	5.662 (1.158-40.921)	0.044 ^a	NA	NA
cTNM	3.705 (2.139-7.056)	0.000 ^a	42.002 (2.913-605.511)	0.006 ^a
mCRM	3.439 (1.562-7.838)	0.003 ^a	NA	NA
mEMVI	2.613 (1.199-5.852)	0.017 ^a	NA	NA
Histological grade	0.229 (0.092-0.496)	0.001 ^a	0.113 (0.020-0.658)	0.015 ^a

^a $P < 0.05$.

CEA: Carcinoembryonic antigen; CA19-9: Carbohydrate antigen 19-9; DIS: The distance between tumor and anal margin; mT: MRI T stage; mN: MRI N stage; cM: Clinical M stage; cTNM: Clinical TNM stage; mCRM: MRI-based circumferential resection margin; mEMVI: MRI-based extramural vascular invasion; OR: Odds ratio; CI: Confidence interval; NA: Not available.

Table 5 Performance of various radiomics predictive models in the training group as evaluated using the Delong test, integrated discrimination improvement index and net reclassification improvement index

Radiomics prediction models	AUC (95%CI)	Delong test P value	IDI (95%CI)	IDI index P value	NRI (95%CI)	NRI index P value
T2WI + T1CE	0.839 (0.757-0.921)					
T2WI	0.817 (0.733-0.901)	0.252	0.081 (0.031-0.131)	0.001	0.510 (0.104-0.865)	0.008
T1CE	0.798 (0.707-0.890)	0.196	0.127 (0.064-0.190)	0.000	0.536 (0.255-1.018)	0.005

AUC: Area under receiver operating characteristic curve; IDI: Integrated discrimination improvement; NRI: Net reclassification improvement; T2WI: T2-weighted imaging; T1CE: Contrast-enhanced T1WI.

combined CR predictive model through logistic regression. The combined CR model demonstrated AUCs of 0.889, 0.889 and 0.894 in the training, internal validation and external validation groups, respectively. Further details are presented in Table 3.

Construction and validation of models

Figure 4 shows the ROC curves of each model in the training, internal validation and external validation groups. The CR model demonstrated the best discrimination ability in each group (Table 3).

Further comparisons were made between the CR, clinical predictive and T2WI + T1CE fusion sequence radiomics predictive models. Based on the training group data, the Delong test showed no significant differences ($P > 0.05$) between the clinical predictive model and T2WI + T1CE fusion sequence radiomics predictive model. The CR model demonstrated a significant difference ($P < 0.05$) compared to the clinical predictive model and T2WI + T1CE fusion sequence radiomics predictive model. NRI and IDI indices further revealed that the CR model had significantly higher predictive ability compared to the clinical predictive model and T2WI + T1CE fusion sequence radiomics predictive model (NRI index > 0 , IDI index > 0 , $P < 0.05$) (Table 6).

The calibration curves of the three models are shown in Figure 5. The CR model had the best calibration ability in the training, internal validation and external validation groups (i.e., the calibration curve was closest to the reference line). The DCA curve is shown in Figure 6. The CR model achieved the highest clinical net benefit compared to the clinical predictive model and T2WI + T1CE fusion sequence radiomics predictive model.

Based on the final results of model construction and validation, the CR model with the best model performance was selected to construct a concise nomogram (Figure 7) and an online interactive dynamic web page nomogram (Figure 8)

Table 6 Performance of the clinical model, T2-weighted imaging + contrast-enhanced T1WI fusion sequence radiomics model, and clinical-radiomics model in the training group, as evaluated using the Delong test, integrated discrimination improvement index, and Net reclassification improvement index

Models	AUC (95%CI)	Delong test <i>P</i> value	IDI (95%CI)	IDI index <i>P</i> value	NRI (95%CI)	NRI index <i>P</i> value
CR model	0.889 (0.824-0.954)					
Clinical	0.804 (0.727-0.881)	0.009	0.210 (0.130-0.290)	0.000	0.588 (0.271-0.904)	0.000
T2WI + T1CE	0.839 (0.757-0.921)	0.019	0.075 (0.026-0.124)	0.002	0.447 (0.164-0.731)	0.002

AUC: Area under receiver operating characteristic curve; IDI: Integrated discrimination improvement; NRI: Net reclassification improvement; CR: Clinical-radiomics; T2WI: T2-weighted imaging; T1CE: Contrast-enhanced T1WI.

for visualization.

DISCUSSION

Noninvasive assessment of the prognosis of RC is challenging and has always been a research hotspot[26,27]. Research has shown that PNI is not only characterized by tumor cell infiltration and growth along the nerves but also involves an interaction between various neurotrophic and chemotactic factors released from tumor cells and the surrounding microenvironment. This process induces tumor invasion, local recurrence, and metastasis, leading to poor prognosis[28-30]. Preoperative prediction of PNI status is helpful for individualized treatment of RC. For example, PNI-positive RC patients should receive more aggressive treatment, such as nCRT[9-12].

The present study constructed radiomics predictive models, clinical predictive models and CR models based on preoperative high-resolution MRI of RC, as well as independent clinical risk factors (cTNM and histological grade), to predict the preoperative PNI status of RC patients. The reliability and repeatability of the established predictive models were analyzed using internal and external validation groups. Compared to the radiomics and clinical predictive models, the CR model had the best discrimination, calibration and clinical net benefit, with stable neutral performance in both the internal and external validation groups.

We constructed three radiomics predictive models based on T2WI and T1CE sequences: T2WI, T1CE and T2WI + T1CE fusion sequence. In the training and internal validation groups, the AUCs of the fusion sequence model were 0.839 (95%CI: 0.757-0.921) and 0.787 (95%CI: 0.650-0.923), which were higher than those of the T2WI and T1CE sequence models. In the external validation group, the AUC of the fusion sequence model was 0.836 (95%CI: 0.735-0.937), which was lower than that of the T1CE sequence model (0.841, 95%CI: 0.752-0.930). Although the AUCs of the fusion sequence models in the training group were higher than those of the T2WI and T1CE sequences, there were no significant differences between the models in the Delong test ($P > 0.05$). The contradictory results may have been due to two reasons: first, the study sample size was not sufficiently large. Further research with larger sample sizes is needed. Second, there are inherent limitations of the Delong test. Although it is widely used to compare models, it may not be sufficiently sensitive to the incremental changes in the predictive ability of the model. Therefore, we also used the NRI and IDI indexes for evaluation[31]. The final results showed that the fusion sequence model had a significantly higher predictive ability compared to the T2WI and T1CE sequence models (NRI index > 0 , IDI index > 0 , $P < 0.05$). Therefore, a CR model was constructed using Rad-score fusion sequences and independent clinical risk factors.

The Rad-score value of the T2WI + T1CE fusion sequence radiomics predictive model consisted of five radiomics features, including one shape feature, two GLCM features, one GLRLM feature and one GLSZM feature. The shape feature is the maximum-2D-diameter-slice based on the original image of the T1CE sequence, which reflects the tumor size. This may be because larger tumors have a higher probability of contact with nerves, leading to a higher probability of PNI[32,33]. The GLCM features include Matthews' correlation coefficient (MCC) based on original T2WI and wavelet transformation of T2WI sequence wavelet-LLL images. The GLCM features mainly reflect the probability of voxel values appearing at a given direction and distance in the spatial arrangement relationship between voxel gray levels of an image. MCC is primarily used to determine the binary classification, and it comprehensively considers true-positive, true-negative, false-positive and false negative cases, making it a balanced indicator. The GLRLM feature is the gray-level nonuniformity normalized (GLNN) based on the T2WI sequence wavelet-LLL image. This feature reflects the spatial arrangement of voxels in the image, and the voxel length with the same gray level continuously appearing in the specified direction. GLNN is primarily used to determine the similarity of gray-level intensity values in the image. The GLSZM feature is the zone entropy (ZE) based on the original T2WI, which reflects the area of continuous voxel values quantified in the spatial arrangement of voxels and gray scales in the image. ZE represents the uncertainty or randomness of the measurement area and grayscale distribution. The higher the value, the greater the nonuniformity of the texture pattern.

Among the five radiomics features, two are wavelet-transformed features, which decompose the original image into different frequency domains and then extract features from each wavelet image individually. Therefore, multi-frequency domain and multi-scale image information can be obtained, allowing the obtained features to reflect the spatial hetero-

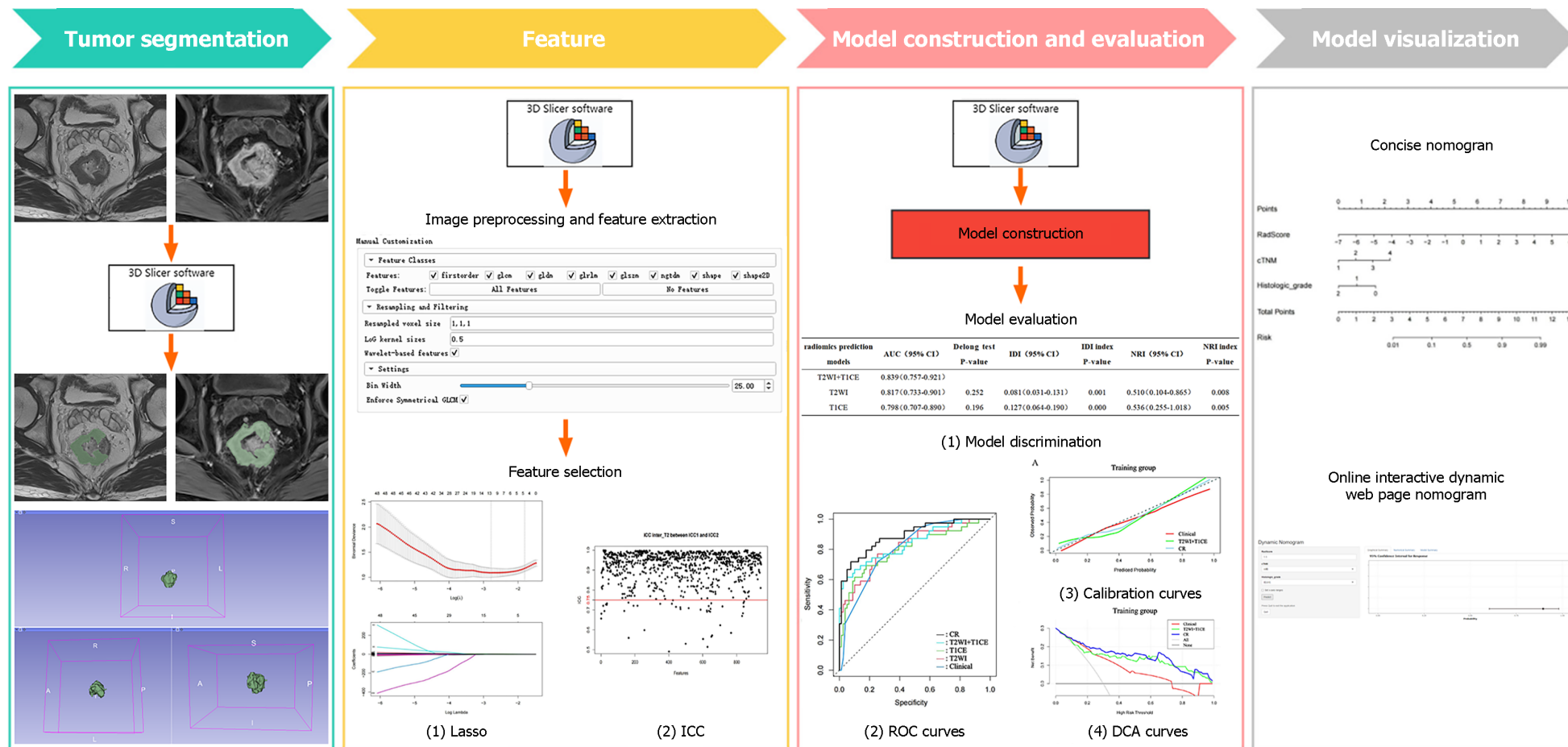


Figure 2 Radiomics workflow.

genity of tumors more effectively. The selected GLCM and GLSZM features of MCC and ZE mainly reflect the heterogeneity of the extracted VOI, which is inconsistent with the specific features extracted by Guo *et al*[23] and Huang *et al* [20]. These findings may be explained by the differences in scanning and reconstruction parameters, as well as inconsistencies between the methods of model construction. Nevertheless, our results were consistent for some of the extracted radiomics features, reflecting tumor heterogeneity. This also confirms the results of previous studies, which found that the higher the tumor heterogeneity, the more aggressive the tumor is likely to be[34]. In addition, the GLRLM feature of GLNN mainly reflects the tumor homogeneity, which is negatively correlated with the Rad-score, confirming our conclusion.

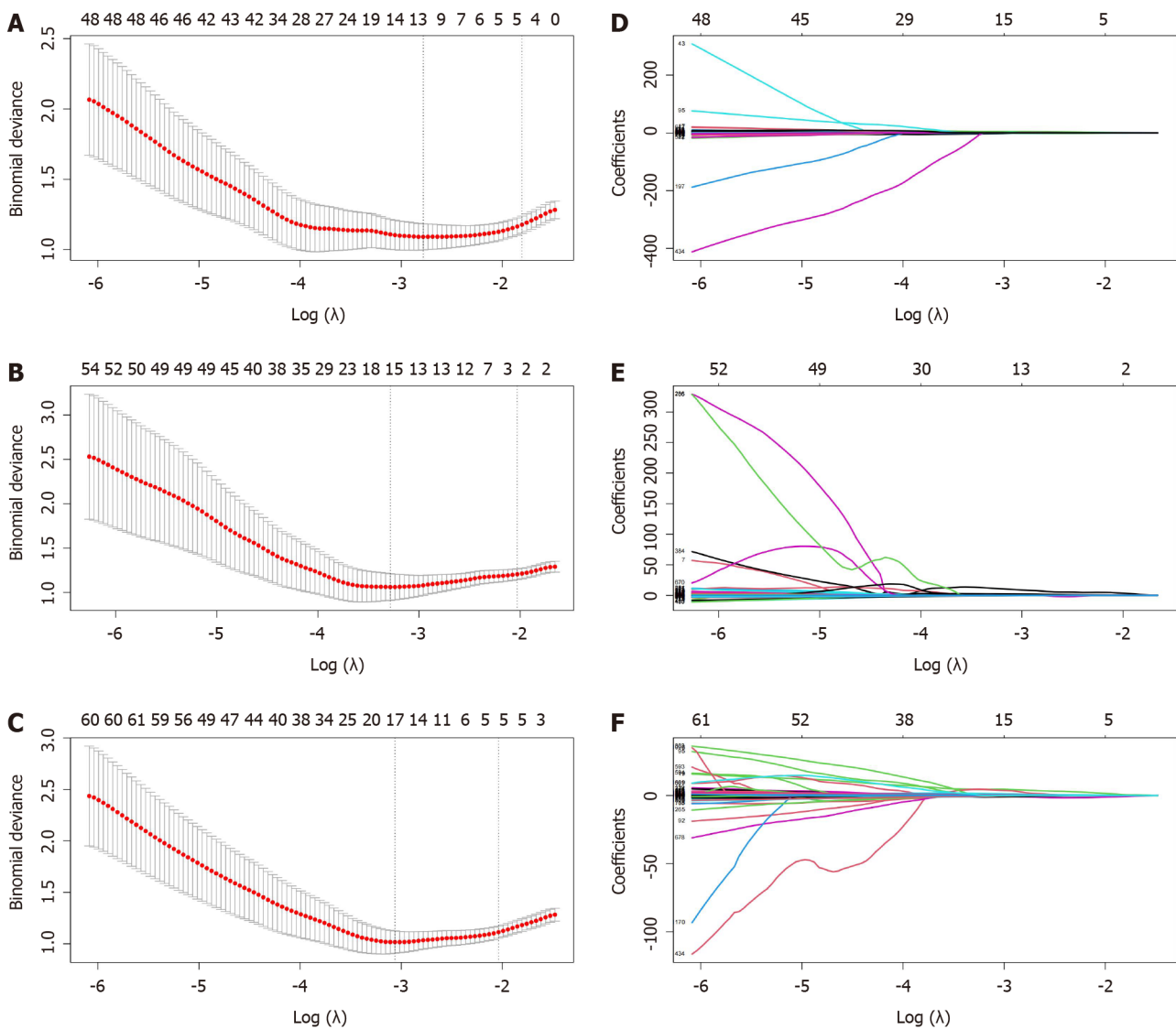


Figure 3 The process of feature selection and dimensionality reduction through least absolute shrinkage and selection operator. A-C: The process of 10-fold crossvalidation penalty parameter λ selection, according to the rule of the simplest model. The abscissa corresponding to the lowest point of model deviation is the optimal λ ; D-F: Each colored line in the variation curve of the characteristic coefficient with value of λ , which was used to determine the non-zero coefficient characteristic parameters based on λ obtained in the upper panel of the figure. T2WI: T2-weighted imaging; T1CE: contrast-enhanced T1WI.

Univariate and multivariate logistic regression analyses of the clinical predictive model showed that cTNM and histological grade were independent risk factors for the PNI status of RC, which is in line with the results of Alotaibi *et al* [32] and Poeschl *et al* [33]. The explanation for these findings may be that a higher TNM stage and lower histological grade correlate with a more malignant and aggressive tumor that is more likely to invade the nerves around the tumors. Previous studies have also shown that a high T stage, high N stage, distant metastasis, positive circumferential resection margin status, positive extramural vascular invasion status, high CEA level (≥ 5 ng/mL), and tumor budding are also independent risk factors for PNI. However, in the present study, the selection of patients and variables was biased due to the study design. Multivariate logistic regression analysis did not reveal significant results. Finally, the clinical predictive model based on cTNM and histological grade was selected, which demonstrated AUCs of 0.804 (95%CI: 0.727-0.881), 0.828 (95%CI: 0.719-0.937) and 0.813 (95%CI: 0.724-0.903) in the training, internal validation and external validation groups, respectively, as well as satisfactory model stability. Compared with the T2WI + T1CE fusion sequence radiomics predictive model, the Delong test showed that there were no significant differences in the differentiation ability among the models. Therefore, the combined CR model was constructed, and showed the best performance. The AUCs of the CR model in the training and internal and external validation groups were 0.889 (95%CI: 0.824-0.954), 0.889 (95% CI: 0.803-0.976) and 0.894 (95%CI: 0.814-0.974), respectively.

Compared with previous similar studies, the present study had certain strengths. First, this study extracted 944 radiomics features from each sequence of the following images: Raw images, Gaussian transformed images, and wavelet transformed images. The number of features was significantly higher than in previous studies, which may reflect the spatial heterogeneity of tumors more effectively. Second, this study used internal and external validation groups to evaluate the models, whereas previous studies were based on a single-center internal validation group, lacking independent external validation. Third, the CR model demonstrated good stability in both the internal and external

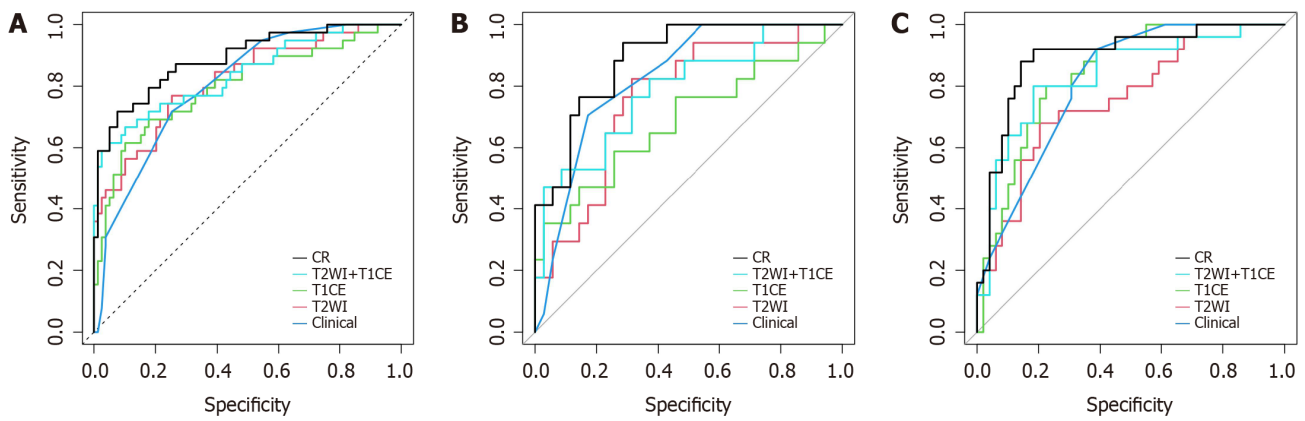


Figure 4 Receiver operating characteristic curves for perineural invasion prediction of different models. A: Receiver operating characteristic (ROC) curves in the training group; B: ROC curves in the internal validation group; C: ROC curves in the external validation group. CR: Clinical-radiomics predictive model; T2WI: T2-weighted imaging; T1CE: Contrast-enhanced T1WI.

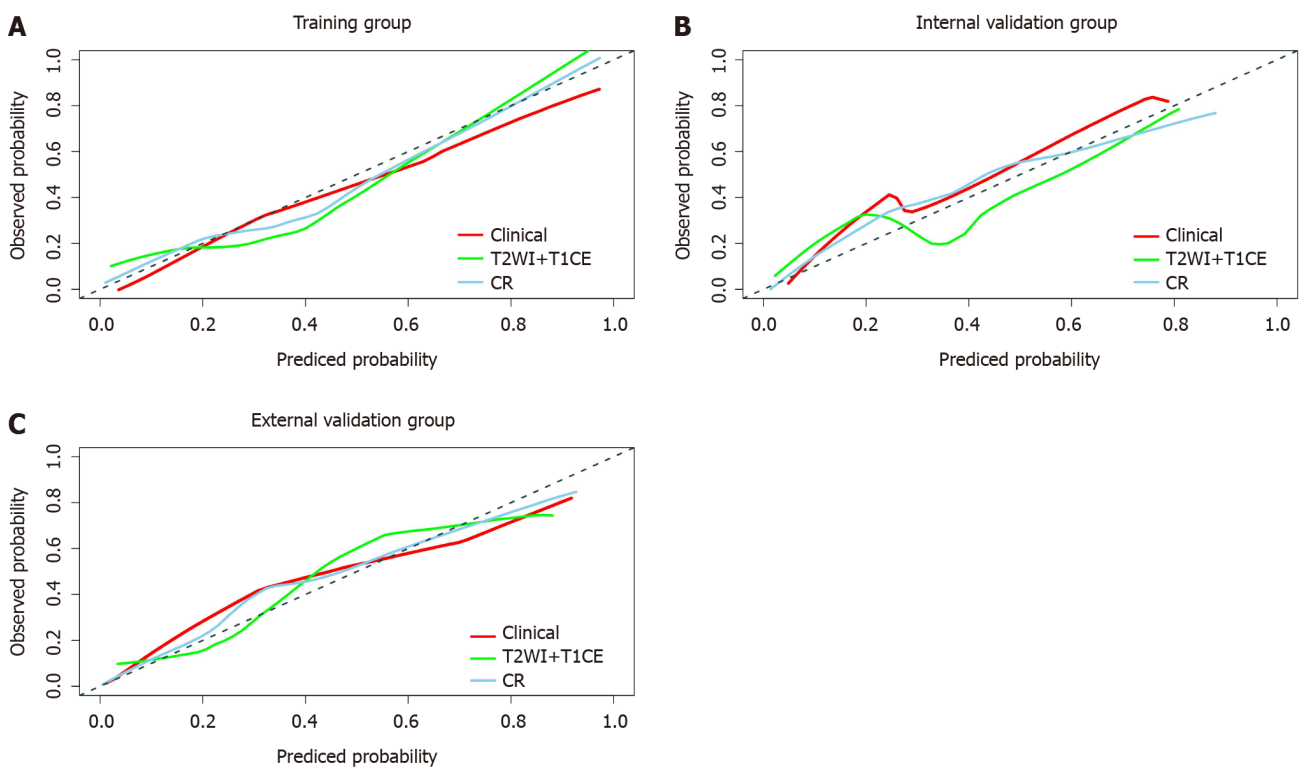


Figure 5 Calibration curves of the clinical model, T2-weighted imaging + Contrast-enhanced T1WI fusion sequence radiomics model and clinical-radiomics prediction model. Diagonal lines serve as reference lines, representing the most suitable model. The clinical-radiomics prediction model shows optimal calibration. A: Calibration curves in the training group; B: Calibration curves in the internal validation group; C: Calibration curves in the external validation group. CR: Clinical-radiomics prediction model; T2WI: T2-weighted imaging; T1CE: Contrast-enhanced T1WI.

validation groups, with greater repeatability than models proposed in previous studies. Fourth, the PNI status of 244 RC patients was evaluated based on HE staining and immunohistochemical analysis of postoperative resection specimens. A previous study demonstrated that immunohistochemical analysis can significantly improve the PNI detection rate, which is 2-3 times higher than the detection rate using HE staining alone[5]. However, some previous studies did not provide a detailed explanation of their specimen analysis methods[13,19,21,22], whereas others evaluated the PNI status based on HE staining only of postoperative specimens[20,23].

There were some limitations to this study. First, this was a retrospective study with possible selection bias. Second, although the external validation group included patients from an independent center based on strict eligibility criteria, further validation studies are needed to reduce the impact of data bias. Third, the VOI was manually delineated layer by layer, which takes a long time in clinical settings and may lead to interobserver variability. Therefore, further studies are needed to determine the feasibility of applying deep learning to automatically delineate the VOI[35,36].

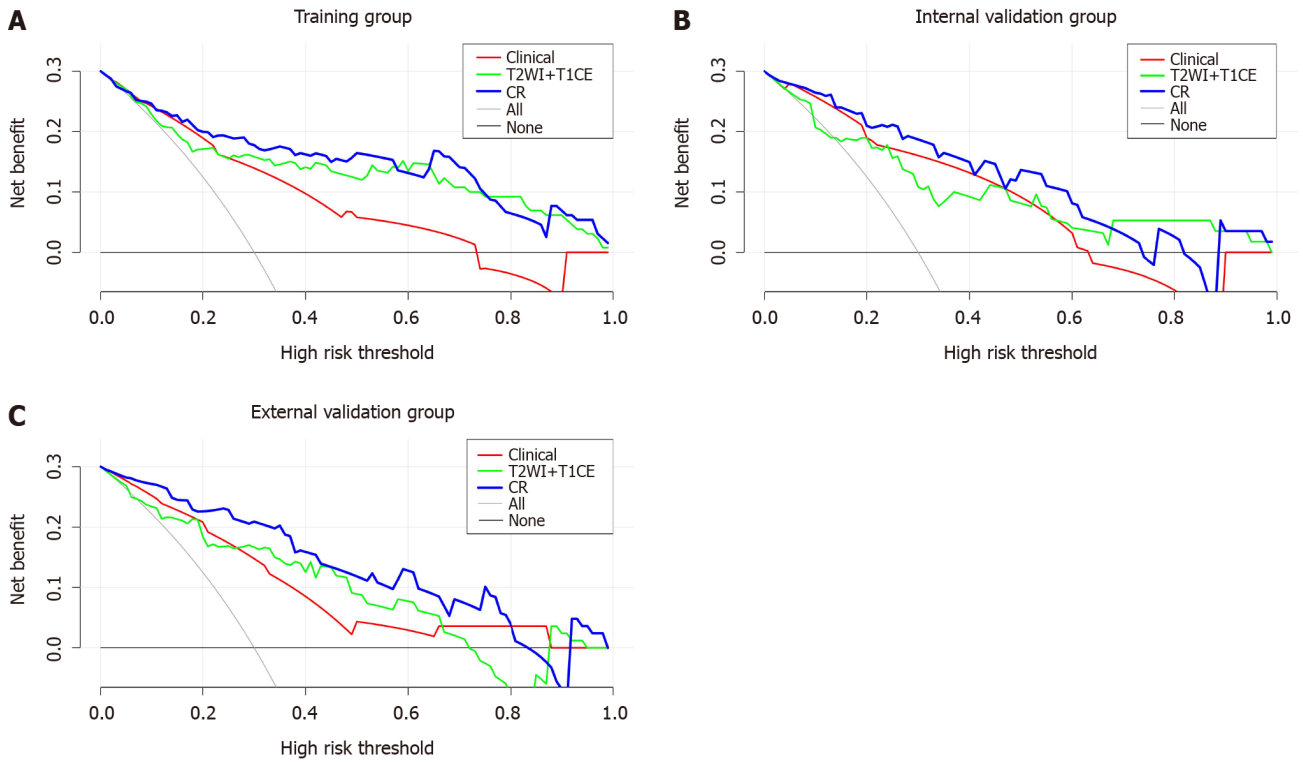


Figure 6 Decision curve analysis of the clinical model, T2-weighted imaging + contrast-enhanced T1WI fusion sequence radiomics model and clinical-radiomics prediction model. The clinical-radiomics prediction model exhibits the greatest net clinical benefit. A: Decision curve analysis (DCA) in the training group; B: DCA in the internal validation group; C: DCA in the external validation group. CR: Clinical-radiomics prediction model; T2WI: T2-weighted imaging; T1CE: Contrast-enhanced T1WI.

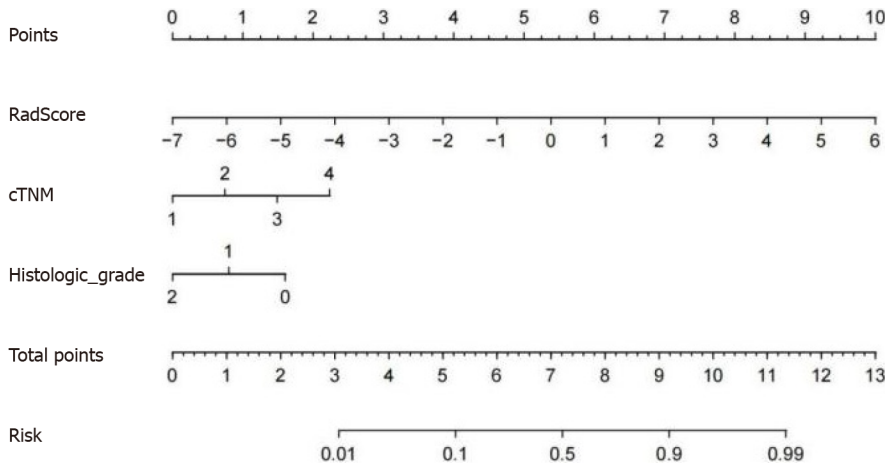


Figure 7 Concise nomogram was developed in the training group. cTNM: clinical TNM.

CONCLUSION

In conclusion, the radiomics model based on preoperative MRI was found to be useful for predicting the PNI status in RC. The CR model combined with the clinical risk factors of PNI was able to predict the PNI status of RC noninvasively before surgery, thereby providing support for the individualized treatment of RC patients.

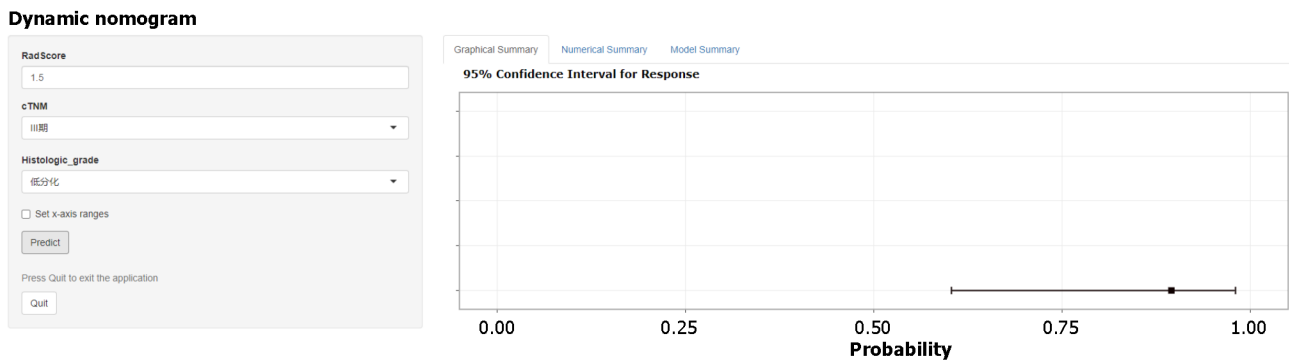


Figure 8 Online interactive dynamic web page nomogram based on the clinical-radiomics model was constructed to predict the perineural invasion status of patients. The Online tool is available at <https://ly1070007554.shinyapps.io/dynnomapp/>.

ARTICLE HIGHLIGHTS

Research background

Perineural invasion (PNI), is a potential pathway for the metastatic spread of rectal cancer (RC), and has been used as an important pathological indicator and independent prognostic factor. Preoperative stratification of RC patients according to PNI status facilitates individualized treatment and improves the prognosis of RC patients.

Research motivation

Nowadays, the preoperative prediction of PNI status is still challenging and needs further study.

Research objectives

To evaluate the usefulness of a model based on preoperative magnetic resonance imaging (MRI) radiomics for predicting PNI status in patients with RC and establishing and validating an optimal nomogram model for predicting PNI status preoperatively in RC patients.

Research methods

We enrolled 244 RC patients from two independent centers from May 2019 to August 2022. The patients from Center 1 were randomly divided into a training group ($n = 118$) and an internal validation group ($n = 52$), whereas 74 patients from Center 2 served as an external validation group. Extracted and selected quantitative radiomics features and clinical risk factors to establish and validate the radiomics predictive model and clinical-radiomics (CR) model.

Research results

We extracted 944 radiomics features from T2-weighted imaging and contrast-enhanced T1-weighted imaging sequences, combined with PNI-related clinical features (clinical TNM and histological grade) to construct the final CR model, and used internal and external validation groups to evaluate the models. The final CR model showed good performance to predict PNI status, the area under the curve of the CR model in the training and internal and external validation groups were 0.889, 0.889 and 0.894, respectively.

Research conclusions

The CR model based on MRI radiomics features and clinical risk factors was able to predict the PNI status of RC noninvasively, showed stable performance, which can provide support for individualized treatment of RC patients.

Research perspectives

Further external verification is needed to optimize the model, and explore the feasibility of applying deep learning to automatically describe volume of interest, reduce the difference between observers, and improve the applicability of the model.

FOOTNOTES

Author contributions: Liu Y data acquisition and analysis, drafting and writing of the manuscript; Sun BJT data collection and data analysis; Zhang C, Li B and Yu XX language editing and revisions to the manuscript; Du Y work concept or design and important revisions to the manuscript; all authors have read and approve the final manuscript.

Institutional review board statement: This study was reviewed and approved by the Ethics Committee of the Affiliated Hospital of North Sichuan Medical College.

Informed consent statement: Patients were not required to give informed consent to the study because the analysis used anonymous clinical data that were obtained after each patient agreed to treatment by written consent.

Conflict-of-interest statement: The authors declare that they have no known competing financial interests or personal relationships that could have appeared to influence the work reported in this paper.

Country/Territory of origin: China

ORCID number: Yan Liu 0009-0006-7654-5463; Xiao-Xuan Yu 0000-0003-1236-5414; Yong Du 0000-0002-8119-3195.

S-Editor: Qu XL

L-Editor: A

P-Editor: Yuan YY

REFERENCES

- 1 Siegel RL, Wagle NS, Cercek A, Smith RA, Jemal A. Colorectal cancer statistics, 2023. *CA Cancer J Clin* 2023; **73**: 233-254
- 2 Edge SB, Compton CC. The American Joint Committee on Cancer: the 7th edition of the AJCC cancer staging manual and the future of TNM. *Ann Surg Oncol* 2010; **17**: 1471-1474
- 3 Liebig C, Ayala G, Wilks JA, Berger DH, Albo D. Perineural invasion in cancer: a review of the literature. *Cancer* 2009; **115**: 3379-3391
- 4 Leijssen LGJ, Dinaux AM, Taylor MS, Deshpande V, Kunitake H, Bordeianou LG, Berger DL. Perineural Invasion Is a Prognostic but not a Predictive Factor in Nonmetastatic Colon Cancer. *Dis Colon Rectum* 2019; **62**: 1212-1221
- 5 van Wyk HC, Going J, Horgan P, McMillan DC. The role of perineural invasion in predicting survival in patients with primary operable colorectal cancer: A systematic review. *Crit Rev Oncol Hematol* 2017; **112**: 11-20
- 6 Knijn N, Mogk SC, Teerenstra S, Simmer F, Nagtegaal ID. Perineural Invasion is a Strong Prognostic Factor in Colorectal Cancer: A Systematic Review. *Am J Surg Pathol* 2016; **40**: 103-112
- 7 Kim CH, Yeom SS, Lee SY, Kim HR, Kim YJ, Lee KH, Lee JH. Prognostic Impact of Perineural Invasion in Rectal Cancer After Neoadjuvant Chemoradiotherapy. *World J Surg* 2019; **43**: 260-272
- 8 Stojkovic Lalosevic M, Milovanovic T, Micev M, Stojkovic M, Dragasevic S, Stulic M, Rankovic I, Dugalic V, Krivokapic Z, Pavlovic Markovic A. Perineural invasion as a prognostic factor in patients with stage I-III rectal cancer - 5-year follow up. *World J Gastrointest Oncol* 2020; **12**: 592-600
- 9 Bakst RL, Lee N, He S, Chernichenko N, Chen CH, Linkov G, Le HC, Koutcher J, Vakiani E, Wong RJ. Radiation impairs perineural invasion by modulating the nerve microenvironment. *PLoS One* 2012; **7**: e39925
- 10 Ceyhan GO, Liebl F, Maak M, Schuster T, Becker K, Langer R, Demir IE, Hartel M, Friess H, Rosenberg R. The severity of neural invasion is a crucial prognostic factor in rectal cancer independent of neoadjuvant radiochemotherapy. *Ann Surg* 2010; **252**: 797-804
- 11 Bosset JF, Calais G, Mineur L, Maingon P, Radosevic-Jelic L, Daban A, Bardet E, Beny A, Briffaux A, Collette L. Enhanced tumorocidal effect of chemotherapy with preoperative radiotherapy for rectal cancer: preliminary results--EORTC 22921. *J Clin Oncol* 2005; **23**: 5620-5627
- 12 Yang Y, Huang X, Sun J, Gao P, Song Y, Chen X, Zhao J, Wang Z. Prognostic value of perineural invasion in colorectal cancer: a meta-analysis. *J Gastrointest Surg* 2015; **19**: 1113-1122
- 13 Chen J, Chen Y, Zheng D, Pang P, Zhang H, Zheng X, Liao J. Pretreatment MR-based radiomics nomogram as potential imaging biomarker for individualized assessment of perineural invasion status in rectal cancer. *Abdom Radiol (NY)* 2021; **46**: 847-857
- 14 Glynne-Jones R, Wyrwicz L, Tiret E, Brown G, Rödel C, Cervantes A, Arnold D; ESMO Guidelines Committee. Rectal cancer: ESMO Clinical Practice Guidelines for diagnosis, treatment and follow-up. *Ann Oncol* 2018; **29**: iv263
- 15 Song JH, Yu M, Kang KM, Lee JH, Kim SH, Nam TK, Jeong JU, Jang HS, Lee JW, Jung JH. Significance of perineural and lymphovascular invasion in locally advanced rectal cancer treated by preoperative chemoradiotherapy and radical surgery: Can perineural invasion be an indication of adjuvant chemotherapy? *Radiother Oncol* 2019; **133**: 125-131
- 16 Sung SY, Kim SH, Jang HS, Song JH, Jeong S, Jung JH, Lee JH. Pathologic Implications of Radial Resection Margin and Perineural Invasion to Adjuvant Chemotherapy after Preoperative Chemoradiotherapy and Surgery for Rectal Cancer: A Multi-Institutional and Case-Matched Control Study. *Cancers (Basel)* 2022; **14**
- 17 Daprà V, Airolidi M, Bartolini M, Fazio R, Mondello G, Tronconi MC, Prete MG, D'Agostino G, Foppa C, Spinelli A, Puccini A, Santoro A. Total Neoadjuvant Treatment for Locally Advanced Rectal Cancer Patients: Where Do We Stand? *Int J Mol Sci* 2023; **24**
- 18 Lambin P, Leijenaar RTH, Deist TM, Peerlings J, de Jong EEC, van Timmeren J, Sanduleanu S, Larue RTHM, Even AJG, Jochems A, van Wijk Y, Woodruff H, van Soest J, Lustberg T, Roelofs E, van Elmpt W, Dekker A, Mottaghy FM, Wildberger JE, Walsh S. Radiomics: the bridge between medical imaging and personalized medicine. *Nat Rev Clin Oncol* 2017; **14**: 749-762
- 19 Li M, Jin YM, Zhang YC, Zhao YL, Huang CC, Liu SM, Song B. Radiomics for predicting perineural invasion status in rectal cancer. *World J Gastroenterol* 2021; **27**: 5610-5621
- 20 Huang Y, He L, Dong D, Yang C, Liang C, Chen X, Ma Z, Huang X, Yao S, Tian J, Liu Z. Individualized prediction of perineural invasion in colorectal cancer: development and validation of a radiomics prediction model. *Chin J Cancer Res* 2018; **30**: 40-50
- 21 Zhang Y, Peng J, Liu J, Ma Y, Shu Z. Preoperative Prediction of Perineural Invasion Status of Rectal Cancer Based on Radiomics Nomogram of Multiparametric Magnetic Resonance Imaging. *Front Oncol* 2022; **12**: 828904
- 22 Yang YS, Qiu YJ, Zheng GH, Gong HP, Ge YQ, Zhang YF, Feng F, Wang YT. High resolution MRI-based radiomic nomogram in predicting perineural invasion in rectal cancer. *Cancer Imaging* 2021; **21**: 40
- 23 Guo Y, Wang Q, Guo Y, Zhang Y, Fu Y, Zhang H. Preoperative prediction of perineural invasion with multi-modality radiomics in rectal cancer. *Sci Rep* 2021; **11**: 9429
- 24 **AJCC Cancer Staging Manual**. 8th ed. Amin MB, Edge SB, Greene FL, editors. 2016. Available from: <http://www.cancerstaging.org>

- 25 **van Griethuysen JJM**, Fedorov A, Parmar C, Hosny A, Aucoin N, Narayan V, Beets-Tan RGH, Fillion-Robin JC, Pieper S, Aerts HJWL. Computational Radiomics System to Decode the Radiographic Phenotype. *Cancer Res* 2017; **77**: e104-e107
- 26 **Bourbonne V**, Schick U, Pradier O, Visvikis D, Metges JP, Badic B. Radiomics Approaches for the Prediction of Pathological Complete Response after Neoadjuvant Treatment in Locally Advanced Rectal Cancer: Ready for Prime Time? *Cancers (Basel)* 2023; **15**
- 27 **De Palma FDE**, Luglio G, Tropeano FP, Pagano G, D'Armiento M, Kroemer G, Maiuri MC, De Palma GD. The Role of Micro-RNAs and Circulating Tumor Markers as Predictors of Response to Neoadjuvant Therapy in Locally Advanced Rectal Cancer. *Int J Mol Sci* 2020; **21**
- 28 **Marchesi F**, Piemonti L, Mantovani A, Allavena P. Molecular mechanisms of perineural invasion, a forgotten pathway of dissemination and metastasis. *Cytokine Growth Factor Rev* 2010; **21**: 77-82
- 29 **Han B**, Guan X, Ma M, Liang B, Ren L, Liu Y, Du Y, Jiang SH, Song D. Stiffened tumor microenvironment enhances perineural invasion in breast cancer *via* integrin signaling. *Cell Oncol (Dordr)* 2023
- 30 **Li X**, Wang Y, Zhai Z, Mao Q, Chen D, Xiao L, Xu S, Wu Q, Chen K, Hou Q, He Q, Shen Y, Yang M, Peng Z, He S, Zhou X, Tan H, Luo S, Fang C, Li G, Chen T. Predicting response to immunotherapy in gastric cancer *via* assessing perineural invasion-mediated inflammation in tumor microenvironment. *J Exp Clin Cancer Res* 2023; **42**: 206
- 31 **Pencina MJ**, D'Agostino RB Sr, D'Agostino RB Jr, Vasan RS. Evaluating the added predictive ability of a new marker: from area under the ROC curve to reclassification and beyond. *Stat Med* 2008; **27**: 157-72; discussion 207
- 32 **Alotaibi AM**, Lee JL, Kim J, Lim SB, Yu CS, Kim TW, Kim JH, Kim JC. Prognostic and Oncologic Significance of Perineural Invasion in Sporadic Colorectal Cancer. *Ann Surg Oncol* 2017; **24**: 1626-1634
- 33 **Poeschl EM**, Pollheimer MJ, Kornprat P, Lindtner RA, Schlemmer A, Rehak P, Vieth M, Langner C. Perineural invasion: correlation with aggressive phenotype and independent prognostic variable in both colon and rectum cancer. *J Clin Oncol* 2010; **28**: e358-60; author reply e361
- 34 **Hardiman KM**, Ulintz PJ, Kuick RD, Hovelson DH, Gates CM, Bhasi A, Rodrigues Grant A, Liu J, Cani AK, Greenson JK, Tomlins SA, Fearon ER. Intra-tumor genetic heterogeneity in rectal cancer. *Lab Invest* 2016; **96**: 4-15
- 35 **Trebeschi S**, van Griethuysen JJM, Lambregts DMJ, Lahaye MJ, Parmar C, Bakers FCH, Peters NHGM, Beets-Tan RGH, Aerts HJWL. Deep Learning for Fully-Automated Localization and Segmentation of Rectal Cancer on Multiparametric MR. *Sci Rep* 2017; **7**: 5301
- 36 **Geng J**, Zhu X, Liu Z, Chen Q, Bai L, Wang S, Li Y, Wu H, Yue H, Du Y. Towards deep-learning (DL) based fully automated target delineation for rectal cancer neoadjuvant radiotherapy using a divide-and-conquer strategy: a study with multicenter blind and randomized validation. *Radiat Oncol* 2023; **18**: 164



Published by **Baishideng Publishing Group Inc**
7041 Koll Center Parkway, Suite 160, Pleasanton, CA 94566, USA
Telephone: +1-925-3991568
E-mail: office@baishideng.com
Help Desk: <https://www.f6publishing.com/helpdesk>
<https://www.wjgnet.com>

